Journal of
Computational and Theoretical Nanoscience
Vol. 7, 1–7, 2010

Modeling Strain Localization Bands in Metal Foams

K. E. Aifantis[1, 2, 3, *], A. Konstantinidis[2], and S. Forest[1]

[1] Centre des Matériaux, Mines ParisTech, Evry 91003, France
[2] Lab Mechanics and Materials, Aristotle University, Thessaloniki, GR 55124, Greece
[3] School of Engineering and Applied Sciences, Harvard, MA 02138, USA

Experimental evidence has documented that during compression of metal foams, deformation is governed by the development of horizontal strain localization bands. Higher-order theories, such as the micromorphic continuum and gradient plasticity have been successfully employed to model experimental data. In the present study after comparing the aforementioned theoretical approaches, an analytical model, using gradient plasticity, is developed that can predict the strain distribution within the foam localization bands. Furthermore, in order to obtain a better understanding of the foam mechanics a numerical approach using cellular automata is used to predict the damage evolution and the stress–strain response during compression; the resulting stress-strain graphs are in very good agreement with experimental data.

Keywords: Foams, Gradient Plasticity, Micromorphic Continuum.

RESEARCH ARTICLE

1. INTRODUCTION

During the past decade metal foams have found use in many industrial applications; particularly in power sources (Ni batteries) and the automotive industry (candidate materials for energy absorption during car crashing). Some of the unique properties that metal foams possess and make them preferable over traditional metallic materials are good stiffness and strength to weight ratios, high impact energy absorption, good sound damping, electromagnetic wave absorption, thermal insulation and non combustibility.[1] Their high stiffness and temperature capability makes them preferable over their counterpart polymer foams and therefore they have found wide use as cores of sandwich beams, plates and shells.

In all of the aforementioned applications the main mechanical aspect that needs to be understood and modeled, in order to optimize the use of foams, is their behavior during deformation. The present study will, therefore, focus on the response of foams during compressive loading. Experimental evidence in this area has revealed that upon compression, strain localization takes place, leading to the formation of multiple horizontal bands, which allow the material to deform at a relatively constant stress, as seen in Figure 1 (see Refs. [1–3]). In the kind of aluminum foams investigated in these references, brittle fracture can take place within these bands, at an early stage, resulting in the collapse of the material. This is especially the case in the rather brittle foams investigated in Refs. [3, 4].

During the past several years various analytical and numerical models have been developed in order to capture this behavior and related size effects.[5, 6] Two particular theoretical frameworks that have been employed are the gradient plasticity theory in Ref. [7] and the micromorphic continuum in Refs. [6, 8]. In the present study after summarizing the similarities and differences between these two theoretical approaches, strain gradient plasticity[9] will be employed to (i) predict analytically the shear strain distribution within a band, (ii) capture numerically the damage evolution and stress–strain response of foams during compression.

2. STRAIN GRADIENT PLASTICITY VERSUS MICROMORPHIC MODELS

2.1. Gradient Plasticity

The difference between gradient plasticity and conventional plasticity is consideration of the gradient of the plastic strain as a state variable. The first gradient model, motivated by the existence of pattern formation during deformation, is that proposed by Aifantis in 1984,[9] according to which the gradient of the plastic strain is simply subtracted

*Author to whom correspondence should be addressed.

 1546-1955/2010/7/001/007 doi:10.1166/jctn.2010.1367

from the classical equivalent flow stress; allowing therefore for a gradient dependent equivalent stress written as

$$\sigma = k(\varepsilon^p) - c\nabla^2\varepsilon^p \tag{1}$$

where $k(\varepsilon^p)$ is the equivalent flow stress under classical plasticity and the constant c is termed the gradient coefficient and is required for dimensional consistency. It is related to an intrinsic material length (ℓ), characteristic of the particular material at hand ($\sqrt{c} = \ell$).

2.2. Micromorphic Model

The micromorphic model can be thought of as being more general, since it not only accounts for the gradient of the plastic strain but for the full gradient. This approach was introduced in the works of Eringen[10] and Mindlin,[11] and has been revisited in.[12] In this section it will be shown that if the micromorphic model is specialized to plastic strain, it reduces to the gradient plasticity model proposed in,[9] aka Equation (1). Letting p be the cumulative plastic strain and introducing the micromorphic plastic strain, ${}^{\chi}p$, which is regarded as an independent degree of freedom in the spirit of Eringen,[10] the energy functional Ψ is defined as

$$\begin{aligned} \rho\Psi(\varepsilon^e, p, {}^{\chi}p, \nabla^{\chi}p) &= \rho\Psi^1(\varepsilon^e, p) + \rho\Psi^2((p - {}^{\chi}p), \nabla^{\chi}p) \\ &= \frac{1}{2}\varepsilon^e C\varepsilon^e + \frac{1}{2}Hp^2 + \frac{1}{2}{}^{\chi}H(p - {}^{\chi}p)^2 \\ &\quad + \frac{1}{2}A\nabla^{\chi}p\cdot\nabla^{\chi}p \end{aligned} \tag{2}$$

where $\rho\Psi_1$ denotes the specific free energy density for a classical material, while $\rho\Psi_2$ is the additional energy contribution that characterizes the micromorphic continuum. Equation (2) implies the following conjugate variable expressions:

$$\begin{aligned} &\sigma = \rho\frac{\partial\Psi}{\partial\varepsilon^e} = \frac{1}{2}\varepsilon^e C\varepsilon^e; \quad R = \rho\frac{\partial\Psi}{\partial p} = (H - {}^{\chi}H)p - {}^{\chi}H{}^{\chi}p; \\ &a = \rho\frac{\partial\Psi}{\partial{}^{\chi}p} = -{}^{\chi}H(p - {}^{\chi}p); \quad b = \rho\frac{\partial\Psi}{\partial\nabla^{\chi}p} = A\nabla^{\chi}p \end{aligned} \tag{3}$$

where ε^e denotes the elastic strain tensor. According to the micromorphic model, the generalized stresses a and b are introduced that are respectively conjugate with ${}^{\chi}p$ and $\nabla^{\chi}p$. They fulfill the following balance equation:

$$a = \mathrm{div}b$$

Inserting the constitutive Eqs. (2) and (3) into the previous balance equation yields:

$$\begin{aligned} a = -{}^{\chi}H(p - {}^{\chi}p) &= \mathrm{div}b = A\mathrm{div}\nabla^{\chi}p = A\Delta^{\chi}p \\ &\Rightarrow p = {}^{\chi}p - A/{}^{\chi}H\Delta^{\chi}p \end{aligned} \tag{4}$$

Equation $(4)_2$ has been postulated in,[13] but is derived here from the micromorphic framework using simple linear constitutive equations.

In order to compare with gradient plasticity, the corresponding yield function is written for the aforementioned micromorphic continuum as:

$$f(\sigma, R) = \sigma_{\mathrm{eq}} - R_0 - R = \sigma_{\mathrm{eq}} - R_0 - {}^{\chi}H{}^{\chi}p + c\Delta^{\chi}p \tag{5}$$

Where σ_{eq} is an equivalent stress measure, which for simple tension gives

$$\sigma = R_0 + {}^{\chi}H{}^{\chi}p - c(H + {}^{\chi}H)\Delta^{\chi}p \tag{6}$$

the coefficient c is of the same nature as in Eq. (1) and is equal to $c = A(H + {}^{\chi}H)/{}^{\chi}H$.

At this stage, an internal constraint can be imposed such that $p \equiv {}^{\chi}p$. Under these conditions, the micromorphic model reduces to the strain gradient formulation,[9] aka Equation (1).

3. DETERMINATION OF LOCALIZATION BAND WIDTH

Although one of the first applications of gradient plasticity was the determination of shear band widths, it has not been applied in such a way to foams. Most gradient plasticity models in this area are concerned with the interpretation of size effects.[7] The micromorphic model, however, has been implemented through the finite element method to provide numerically the stain distribution inside foam localization bands.[3,6] In this section it will be shown that the gradient plasticity framework can be used so as to provide analytic solutions for the strain distribution inside bands.

To account for the presence of localization bands the yield function must allow for softening, therefore it is defined as

$$f(\sigma) = \sqrt{J_2^2 + \alpha I^2} - R(p) + c\nabla^2 p \tag{7}$$

where p is the plastic strain multiplier, c the gradient coefficient, and $R(p)$ is the hardening function. The first and second invariants of the stress tensor respectively are I and J_2. The model corresponds to the elliptic criterion used for compressible plasticity and applied to metallic foams in Refs. [14–15]. It should be noted that elimination of the last term in Eq. (7) gives us a yield function for classical plasticity.

The plastic strain rate may now be defined as

$$\dot{\varepsilon}^p = \dot{p}\frac{\partial f}{\partial\sigma} \Rightarrow \dot{\varepsilon}^p = \dot{p}\frac{1}{\tau}\left(\frac{3}{2}\sigma^{\mathrm{dev}} + \alpha(tr\sigma)1\right) \tag{8}$$

where p is the cumulative plastic strain such that $\sigma : \dot{\varepsilon}^p = \dot{p}\sigma_{eq}$.

For compression, Eq. (7) can be re-written as

$$\begin{aligned} f(\sigma) &= \sqrt{\sigma^2 + \alpha\sigma^2} - R(p) + c\nabla^2 p \\ &= \sqrt{1+\alpha}|\sigma| - R(p) + c\nabla^2 p \\ &\Rightarrow \sqrt{1+a}|\sigma| = R - c\nabla^2 p = R_0 + Hp - cp_{,yy} \end{aligned} \tag{9}$$

where the hardening function has been defined as $R(p)=R_0+Hp$.

The resulting equilibrium conditions are:

$$\sigma_{yy,y}=0\Rightarrow\sigma=\text{constant} \tag{10}$$

$$Hp_{,y}-cp_{,yyy}=0\Rightarrow p_{,yyy}=\frac{H}{c}p_{,y} \tag{11}$$

When the hardening modulus, H, is negative (softening behavior associated with shear band formation), Eq. (11) can be integrated to give us the plastic strain distribution as

$$p(y)=A\cos(\omega y)+B\sin(\omega y)+C \tag{12}$$

where, $\omega^2=|H|/c>0$, and A, B, C are constants of integration.

Letting the plastic strain at the endpoints of the localization band equal to zero, and imposing a maximum at $y=0$ the following conditions are developed:

$$p(L)=p(-L)=0;\quad p'(0)=0 \tag{13}$$

It is noted here that the band width is $2L$.

Combination of Eq. (13) with Eq. (12) gives

$$A\cos(\omega L)+B\sin(\omega L)+C=0$$
$$A\cos(\omega L)-B\sin(\omega L)+C=0$$
$$A\omega\sin(0)+B\omega\cos(0)=0$$

which allows the determination of B and A as: $B=0$; $A=-C/(\cos\omega L)$.

Since, however, a maximum has been imposed at $y=0$ an additional condition is present: $p_{\max}=p(0)=A+C$, which allows the determination of A and C as:

$$A=-\frac{p_{\max}}{1-\cos(\omega L)},\quad C=\frac{p_{\max}\cos(\omega L)}{1-\cos(\omega L)}$$

Inserting the above expressions in Eq. (12) allows for the complete expression for p as

$$p(y)=p_{\max}\frac{\cos(\omega y)-\cos(\omega L)}{1-\cos(\omega L)},\quad \text{for } -L\le y\le L \tag{14}$$

where $2L=$cell size. In order to evaluate Eq. (14) it remains to define the gradient coefficient c. In Refs. [16–17] it was derived that

$$c=(\lambda+H)\frac{d^2}{10}$$

where λ is taken to be the elastic modulus, H the hardening modulus, and d is the cell size (i.e., $d=2L$). It should be said here that the plastic strain profile (Eq. 14), derived from strain gradient plasticity, is closely related to the one found in Ref. [6] within the context of the micromorphic continuum; this was expected from the discussion in the previous Section 2.2. Finally, by allowing for various values of the maximum strain $p_{\max}$, and taking the material parameters as $E=140$ MPa and $d=0.004$ as provided in Ref. [6], while letting H be -6.8 MPa, Eq. (14) is plotted to show the strain distribution inside a band (Fig. 2) for various values of $p_{\max}$.

Before concluding this analytic section it is of interest to show a type of size effect that can be obtained for the strain distribution inside bands of different widths. Integration of the strain distribution Eq. (14) over the band width gives the total strain that is applied on the foam as

$$\varepsilon=\frac{1}{2L}\int_{-L}^{L}p_{\max}\frac{\cos(\omega y)-\cos(\omega L)}{1-\cos(\omega L)}dy$$
$$\Rightarrow\varepsilon=-\frac{p_{\max}}{2L\omega}\csc\left(\frac{\omega L}{2}\right)^2[\omega L\cos(\omega L)-\sin(\omega L)] \tag{15a}$$

Equation (15a) can be solved for $p_{\max}$, so as to obtain the maximum strain within the band ($p_{\max}$) as a function of the applied strain (ε) that results from the applied stress σ:

$$p_{\max}=-\frac{\varepsilon\omega\sin(\omega L/2)^2}{\omega L\cos(\omega L)-\sin(\omega L)} \tag{15b}$$

Inserting Eq. (15b) in Eq. (14) gives the strain distribution within the band as a function of the total applied strain

$$p(y)=\frac{\varepsilon\omega(\cos(\omega L)-\cos(\omega y))}{2\omega L\cos(\omega L)-2\sin(\omega L)},\quad \text{for } -L\le y\le L \tag{15c}$$

Equation (15c) allows us to obtain the strain distribution within the bands, for the same applied strain but for different band widths, as shown in Figure 3.

Finally, the applied stress in the foam can be found by Eq. (9) which can be re-written based on Eq. (14) as

$$\sqrt{1+\alpha}\sigma=R_0+Hp-cp_{,yy}$$
$$=R_0+Hp_{\max}\frac{\cos(\omega y)-\cos(\omega L)}{1-\cos(\omega L)}$$
$$-Hp_{\max}\frac{\cos(\omega y)}{1-\cos(\omega L)}$$

Therefore the flow stress in the foam is a constant given by the expression:

$$\Rightarrow\sigma=\left(R_0-Hp_{\max}\frac{\cos(\omega L)}{1-\cos(\omega L)}\right)\Big/\sqrt{1+\alpha} \tag{16}$$

To further understand the overall effects that deformation has on foams the damage evolution during compression will be modeled in the sequel.

4. STRESS–STRAIN RESPONSE DURING COMPRESSION

4.1. Theoretical Formulation

In Figure 1 the experimental response during compression of a Al foam is displayed. It can be seen that after the material yields, deformation occurs at a relatively constant stress

RESEARCH ARTICLE

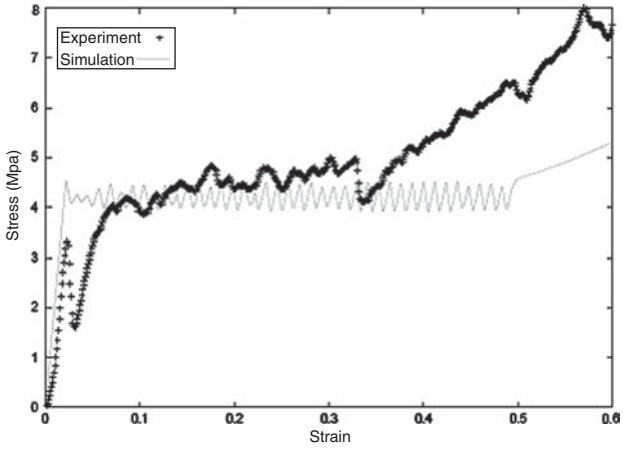

Fig. 1. Stress–strain response of an Al foam during compression, after Ref. [6].

due to band formation. In the experiment this "plateau" stress is not exactly constant but increases slowly with some variation corresponding to the formation and saturation of localization bands. In the finite element simulation shown in Figure 1 this variation appears to be periodic; this is due to the fact that in Ref. [6] randomness effects were not accounted for. In the present study, we shall try to capture the slight increase of this "plateau" stress by allowing the crushing strength of each cell in the foam to vary, i.e., the crushing strength will be treated as a random variable.

During the compression of porous materials, in general, three stages can be identified: (i) elastic bending of the walls, (ii) formation and propagation of localized strain bands, (iii) individual cell collapse that leads to compaction. To capture this behavior the stress–strain response is defined, according to Ref. [18] as

$$\sigma=\begin{cases} M\varepsilon & \text{for } \varepsilon<\varepsilon_c \\ M\varepsilon_c\left[e^{(\varepsilon_{\text{comp}}(\varepsilon-\varepsilon_c))/(\varepsilon_{\text{comp}}-\varepsilon)}-\varepsilon_0(\varepsilon-\varepsilon_c)\right] & \text{for } \varepsilon>\varepsilon_c \end{cases} \tag{17}$$

where M is the elastic modulus, σ_c the crushing threshold, and ε_0 the parameter determining the extension of the softening regime given as in Ref. [18]

$$\varepsilon_0=\frac{1}{\varepsilon_{\text{crush}}}[e^{(\varepsilon_{\text{comp}}\varepsilon_{\text{crush}})/(\varepsilon_{\text{comp}}\varepsilon_{\text{crush}}-\varepsilon_c)}-1] \tag{18}$$

These parameters can be better seen in Figure 4.

It follows that as individual cells collapse, their neighbors are affected, therefore an interaction stress is defined, between adjacent cells i and j, as

$$\sigma_{ij}=D_{ij}(\varepsilon_i-\varepsilon_j) \tag{19}$$

where $D_{ij}=\beta_{ij}(\sigma_c/\varepsilon_{\text{crush}})$ and β_{ij} is the coupling constant that depends on the orientation with respect to the compression direction.

The quasi-static cell balance, which is the equilibrium equation for our system is written as[19]

$$\sigma_{\text{ext}}-\sigma(\varepsilon_i)-\sum_j D_{ij}(\varepsilon_i-\varepsilon_j)=0 \tag{20}$$

Coarse graining now the above equation, over a large volume that is comparable to the cell size d, gives a strain-gradient type equilibrium condition for the two-dimensional case:[18]

$$\sigma_{\text{ext}}-\sigma(\varepsilon(r))+\nabla[D\nabla\varepsilon(r)]=0,\quad D=d^2\frac{\sigma_c}{\varepsilon_c}\begin{bmatrix}\beta_p & 0\\ 0 & \beta_n\end{bmatrix} \tag{21}$$

where β_p and β_n denote the coupling constants at the parallel and normal to the compression direction, respectively.

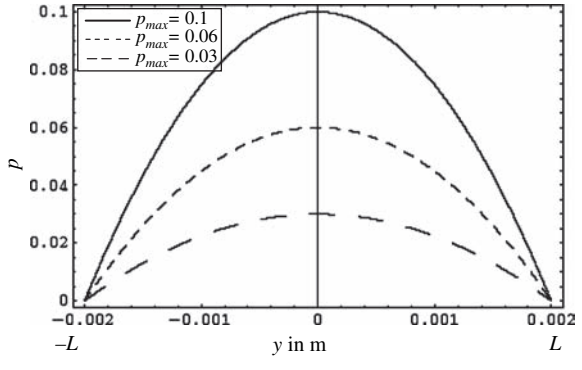

Fig. 2. Strain profile within localization band; the constants in Eq. (14) are taken as: $2L=d=0.004$ m, $E=150$ MPa, $H=-6.8$ MPa, while $p_{\max}$ is varied.

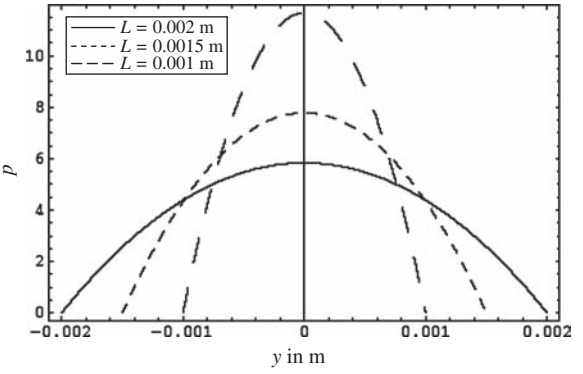

Fig. 3. Strain profile within band for different cell sizes ($2L=d$); $E=150$ MPa, $H=-6.8$ MPa; the total applied strain for all curves is the same $\varepsilon=0.004$.

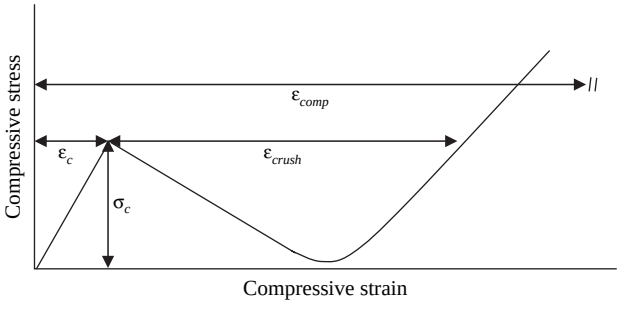

Fig. 4. Stress–strain response of a hypothetical material.

RESEARCH ARTICLE

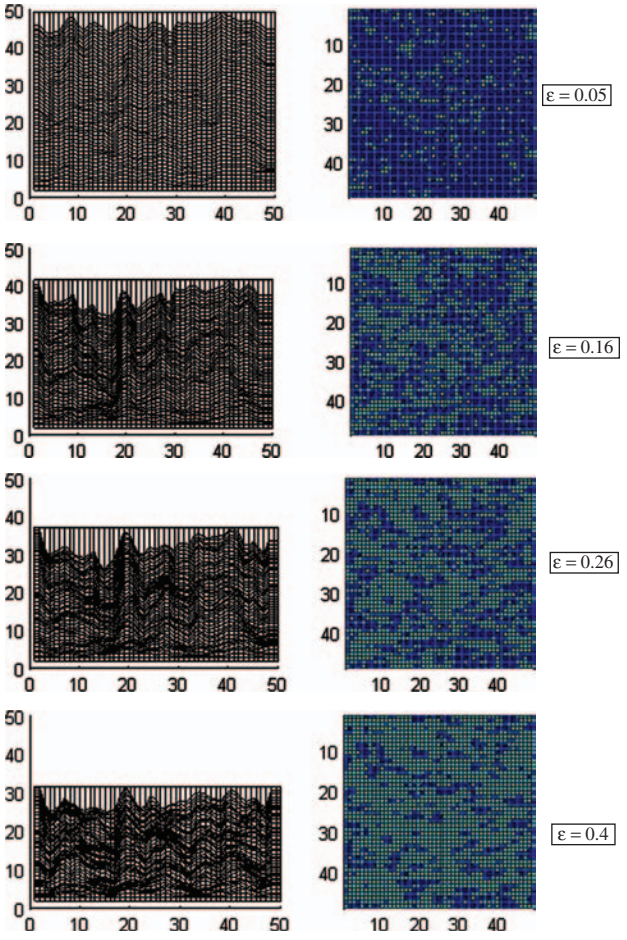

Fig. 5. Simulation results for an Al foam with large randomness ($m=8.9$ and $h=3.27$) in the crushing thresholds. The left images depict the deformation of the simulated foam, while the right images show the particular damage in each foam cell as the strain increases; damaged (light blue), versus undamaged (dark blue).

4.2. Simulation Results

Numerical simulations of the constitutive Eq. (20) were performed using a cellular automaton with 50×50 cells. The local heterogeneities in the properties of real cellular materials are taken into account in the simulations by assigning random variations of the crushing thresholds of the cells, i.e., the thresholds σ_C are considered independent random variables obeying a Weibull distribution with scale and shape parameters m and h respectively, leading to specific values for the mean $\langle\sigma_C\rangle$ and variance $\delta\sigma_c$.

The system is loaded by increasing the external strain ε_{ext} from zero in small steps $\Delta\varepsilon_{\text{ext}}$, Since experiments for metal foams are usually performed with strain control, in the present simulations the system is loaded by increasing the external strain ε_{ext} in small steps $\Delta\varepsilon_{\text{ext}}$ (starting of course with $\varepsilon_{\text{ext}}=0$). In each of the cells where the local (external plus internal) stress exceeds the local crushing threshold, the local strain is increased by a small constant amount $\delta\varepsilon$. Then, new internal stresses are computed for all sites and it is checked again whether the sum of the external and internal stresses exceeds the local crushing threshold. The local strain at the now "damaged" sites is again increased, etc. This is repeated until the system has reached a new stable configuration. Then the external strain is increased again and so on.

It should be noted that initially the "local" modulus M is taken to be constant and equal to the modulus of Al (70 GPa) for all n (50×50) cells. The "effective" modulus can be defined as

$$M_{\text{eff}}=\frac{n}{\sum_n \frac{1}{M_i}} \tag{22}$$

providing an "effective" external stress for all cells as

$$\sigma_{\text{ext}}=M_{\text{eff}}(\varepsilon_{\text{ext}}-\varepsilon_p) \tag{23}$$

After each run where the local strain of a "damaged" site is increased by the small constant amount $\delta\varepsilon$, the overall change in the "effective" strain ε_p is $\delta\varepsilon/n$. Then, the new moduli of the damaged sites are calculated as $M_i=e^{\varepsilon_i}$, where ε_i is the new local stress of cell i.

In Figure 5 the simulation results are shown for the case where the random variables of the Weibull distribution assume the values measured in the experiments by Blazy et al.:[20] $m=8.9$ and $h=3.27$. These values imply a large randomness which leads to the formation of multiple damage zones that cannot be depicted individually by the simulation. It should be noted that the simulation time was approximately 20 seconds for the case of a system with 50×50 cells, while it was approximately double for the case of a system with 100×100 cells.

A plot of the effective stress versus the effective strain computed in this way for the case of large randomness is given in Figure 6. For comparison the experimental data of Blazy et al.[20] are also plotted in the same graph. The

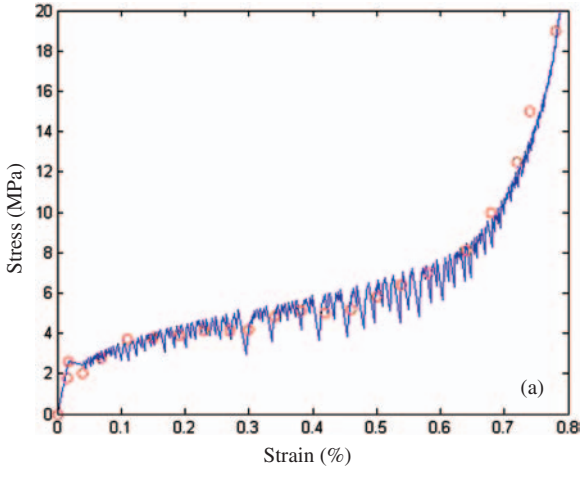

Fig. 6. Effective stress–strain simulation results (blue line) for an Al foam with large randomness ($m=8.9$ and $h=3.27$) compared with experimental Al foam data by Blazy et al.[20] (red circles).

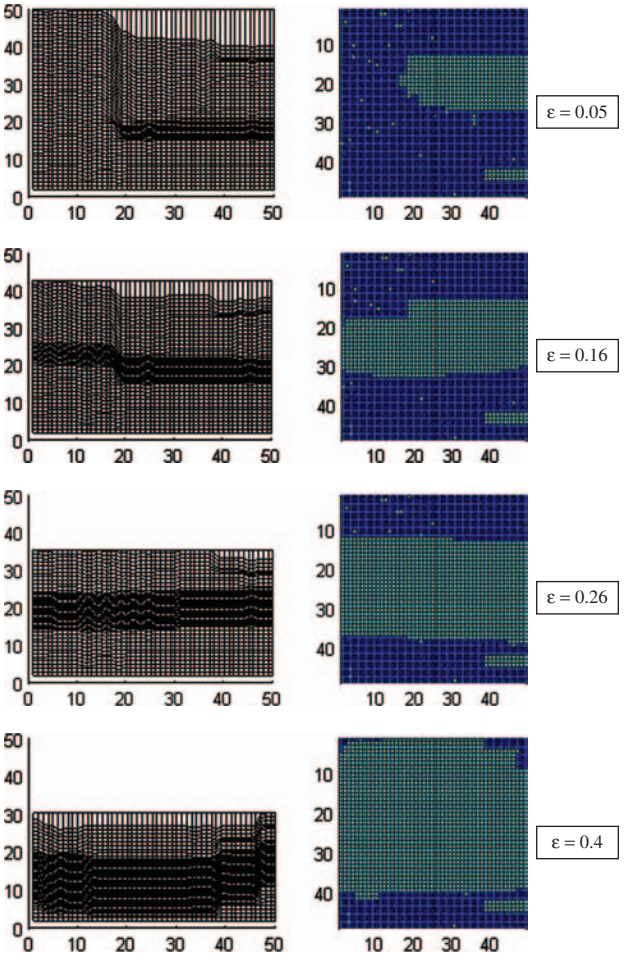

Fig. 7. Simulation results for an Al foam with small randomness ($m=8.9$ and $h=8$) in the crushing thresholds. The left images depict the deformation of the simulated foam, while the right images show the particular damage in each foam cell as the strain increases; damaged (light blue), versus undamaged (dark blue). The evolution and propagation of single bands can be seen for small randomness.

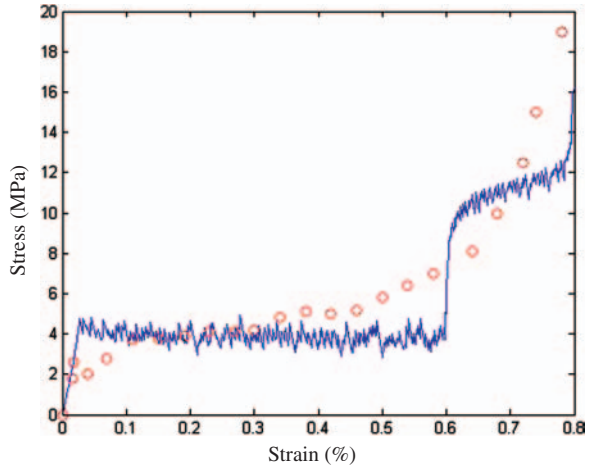

Fig. 8. Effective stress–strain simulation results (blue line) for an Al foam, for relatively small randomness ($m=8.9$ and $h=8$), compared with Al foam experimental data by Blazy et al.[20] (red circles).

agreement of the simulation with the experiment is quite remarkable and is an indication that the proposed model captures adequately the behavior of metallic foams during compression.

In order to compare the present numerical approach with the finite element approach of, Ref. [6] in which random effects were not accounted for, the cellular automaton simulation is re-run for a small randomness (e.g., $m=8.9$ and $h=8$), which implies the formation and propagation of a single damage zone (Fig. 7). As expected, in this case, the simulation gives a plateau stress (Fig. 8) similar to that of Figure 1,[6] and agreement with the experimental results is not observed.

It should be noted that the serrations observed in the stress–strain plots (Figs. 6 and 8) result from the fact that the cellular automaton is strain-controlled. A stress-controlled cellular automaton simulation with high randomness for the crushing threshold has also yielded to agreement with experimental data.[21]

In concluding it is noted that the numerical approach presented here can be modified to model deformation at the nanoscale, since experimental evidence[22] suggests that deformation in nanocrystals is governed through shear band formation. In Ref. [22] it is shown that once nanocrystalline Fe-10% Cu alloys yield, plastic deformation is carried out at a constant stress, i.e., a plateau stress is observed similar to that in Figure 1 and 8. However, unlike as in Figures 1 and 8, re-hardening does not occur in nanomaterials, hence the constitutive Eq. (20) used in the numerical approach must be modified so as to account for perfect plasticity after yielding. This task is currently being considered.

Acknowledgments: The authors are grateful for the support of the European Commission through the RTN-DEFINO (HPRN-CT-2002-00198) under which this work was initiated. K. E. Aifantis and A. Konstantinidis are grateful to the ERC Starting-Grant No. 211166 (MINATRAN) for its support to finalize this work.

References

1. L. J. Gibson and M. F. Ashby, Cellular Solids, Cambridge University Press **(1998)**.
2. H. Bart-Smith, A. F. Bastawros, D. R. Mumm, A. G. Evans, D. J. Sypeck, and H. N. G. Wadley, *Acta Mater.* 46, 3583 **(1998)**.
3. J. S. Blazy, A. Marie-Louise, S. Forest, Y. Chastel, A. Pineau, A. Awade, C. Grolleron, and F. Moussy, *Int. J. Mech. Sci.* 46, 217 **(2004)**.
4. A.-H. Benouali, L. Froyen, T. Dillard, S. Forest, and F. N'Guyen, *J. Matls Sci.* 40, 5801, **(2005)**.
5. P. R. Onck, E. W. Andrews, and L. J. Gibson, *Int. J. Mech. Sci.* 43, 681 **(2001)**.
6. S. Forest, J. S. Blazy, Y. Chastel, and F. Moussy, *J. Mat. Sci.* 40, 5903 **(2005)**.
7. C. Chen and N. A. Fleck, *J. Mech. Phys. Sol.* 50, 955 **(2002)**.
8. T. Dillard, S. Forest, and P. Ienny, *Eur. J. Mech. A/Sol.* 25, 526 **(2006)**.
9. E. C. Aifantis, *J. Eng. Mater. Technol.* 106, 326 **(1984)**.

RESEARCH ARTICLE

10. R. Mindlin, *Arch. Rat. Mech. Anal.* 16, 51 **(1964)**.
11. A. Eringen and E. Suhubi, *Int. J. Eng. Sci.* 2, 189 **(1964)**.
12. S. Forest and R. Sievert, *Acta Mechanica* 160, 71 **(2003)**.
13. R. A. B. Engelen, M. G. D. Geers, and F. P. T. Baaijens, *Int. J. Plast.* 19, 403 **(2003)**.
14. V. S. Deshpande and N. A. Fleck, *J. Mech. Phys. Sol.* 48, 1253 **(2000)**.
15. X. Badiche, S. Forest, T. Guibert, Y. Bienvenu, J.-D. Bartout, P. Ienny, M. Croset, and H. Bernet, *Mat. Sci. Eng. A* A289, 276 **(2000)**.
16. E. C. Aifantis, *Int. J. Eng. Sci.* 33, 2161 **(1995)**.
17. J. Ning and E. C. Aifantis, Constitutive Laws of Plastic Deformation, edited by A. S. Krausz and K. Krausz, Academic Press.
18. E. C. Aifantis, *Int. J. Plasticity* 3, 211 **(1987)**.
19. M. Zaiser and E. C. Aifantis, Modeling the crushing of a cellular material, *Proc. 6th Nat. Cong. of Mechanics*, edited by E. C. Aifantis and A. N. Kounadis, Giahoudi-Giapouli Publ., Thessaloniki **(2001)**, Vol. 3, p.102.
20. J.-S. Blazy, A. Marie-Louise, S. Forest, Y. Chastel, A. Pineau, A. Awade, C. Grolleron, and F. Moussy, *Int. J. Mech. Sci.* 46, 217 **(2004)**.
21. K. E. Aifantis, A. A. Konstantinidis, and M. Zaiser, Damage evolution in foams, *Proc. of 4th Int. Conf. on Multiscale Materials Modeling (MMM2008)*, edited by A. El Azab **(2008)**, in press.
22. J. E. Carsley, W. W. Milligan, X. H. Zhu, and E. C. Aifantis, *Scripta Mater.* 36, 727 **(1997)**.

Received: 19 September 2008. Accepted: 2 November 2008.